Structural Determinants and Mechanism of Mammalian CRM1 Allostery

Nicole Dölker,[1,8,9] Clement E. Blanchet,[3,8] Béla Voß,[1,8] David Haselbach,[2,8] Christian Kappel,[1,10] Thomas Monecke,[4] Dmitri I. Svergun,[3] Holger Stark,[2,5] Ralf Ficner,[4] Ulrich Zachariae,[6,7] Helmut Grubmüller,[1,*] and Achim Dickmanns[4,*]

[1]Abteilung für Theoretische und Computergestützte Biophysik
[2]Dreidimensionale Kryo-Elektronenmikroskopie
Max-Planck-Institut für Biophysikalische Chemie, Am Faßberg 11, 37077 Göttingen, Germany
[3]European Molecular Biology Laboratory, Hamburg Unit, EMBL c/o DESY, Notkestraße 85, 22603 Hamburg, Germany
[4]Abteilung für Molekulare Strukturbiologie
[5]Abteilung für Molekulare Kryo-Elektronenmikroskopie
Institut für Mikrobiologie und Genetik, Göttinger Zentrum für Molekulare Biowissenschaften (GZMB), Georg-August-Universität Göttingen, Justus-von-Liebig-Weg 11, 37077 Göttingen, Germany
[6]Division of Computational Biology, College of Life Sciences
[7]Division of Physics, School of Engineering, Physics and Mathematics
University of Dundee, Dundee DD1 5EH, UK
[8]These authors contributed equally to this work
[9]Present address: Centro Nacional de Investigaciones Oncológicas, C/ Melchor Fernández Almagro, 3, 28029 Madrid, Spain
[10]Present address: Konrad-Adenauer-Straße 75, 69207 Sandhausen, Germany
*Correspondence: hgrubmu@gwdg.de (H.G.), adickma@gwdg.de (A.D.)
http://dx.doi.org/10.1016/j.str.2013.05.015

SUMMARY

Proteins carrying nuclear export signals cooperatively assemble with the export factor CRM1 and the effector protein RanGTP. In lower eukaryotes, this cooperativity is coupled to CRM1 conformational changes; however, it is unknown if mammalian CRM1 maintains its compact conformation or shows similar structural flexibility. Here, combinations of small-angle X-ray solution scattering and electron microscopy experiments with molecular dynamics simulations reveal pronounced conformational flexibility in mammalian CRM1 and demonstrate that RanGTP binding induces association of its N- and C-terminal regions to form a toroid structure. The CRM1 toroid is stabilized mainly by local interactions between the terminal regions, rather than by global strain. The CRM1 acidic loop is key in transmitting the effect of this RanGTP-induced global conformational change to the NES-binding cleft by shifting its population to the open state, which displays enhanced cargo affinity. Cooperative CRM1 export complex assembly thus constitutes a highly dynamic process, encompassing an intricate interplay of global and local structural changes.

INTRODUCTION

In contrast to prokaryotic cells, eukaryotic cells reveal a high degree of spatial compartmentalization into membrane-engulfed entities. This, for instance, enables a strict spatiotemporal separation of cellular processes such as transcription, occurring in the nucleus, and translation in the cytoplasm. Transport between the nucleus and the cytoplasm proceeds through nuclear pore complexes (NPC) and depends on specialized transport systems. Macromolecules exceeding 30–40 kDa require the aid of karyopherins (KAPs) as mediators to pass the NPC efficiently (Chook and Süel, 2011; Cook and Conti, 2010).

The majority of KAPs are members of a superfamily named after Importin-β (Impβ), the first receptor identified (Görlich et al., 1997; Radu et al., 1995). They are divided into importins and exportins according to the direction of cargo transport. Their common biochemical properties are the capability to interact with the NPC and bind to the small GTPase Ran (Ras-related nuclear antigen). The asymmetric distribution of the Ran-regulating factors with the Ran guanine-nucleotide exchange factor (RanGEF) residing in the nucleus and the Ran GTPase activating protein (RanGAP) located in the cytoplasmic compartment ensures that nuclear Ran predominantly occurs in its GTP-bound form. In contrast to the cytoplasmic, GDP-bound form of Ran, RanGTP can bind to KAPs. RanGTP binding modulates the affinity of KAPs for cargo and thereby enforces directionality of transport.

On a structural level, all members of the Impβ superfamily share a common arrangement of about 20 building blocks, so-called HEAT repeats (Kobe et al., 1999), each consisting of two antiparallel α helices connected by a loop. Their consecutive arrangement results in an overall superhelical shape resembling a solenoid (Fontes et al., 2000). In exportins, RanGTP promotes cargo binding predominantly by interacting simultaneously with receptor and cargo, as for instance seen in Exportin-t, Exportin5, or Cse1p/CAS (Cook et al., 2005, 2009; Matsuura and Stewart, 2004; Okada et al., 2009). In contrast, the export receptor CRM1 (chromosome region maintenance 1), which recognizes the majority of proteins destined for export (Hutten and Kehlenbach, 2007), displays no direct interaction of Ran and cargo. CRM1 in the cargo-bound state exhibits a toroidal, compact,
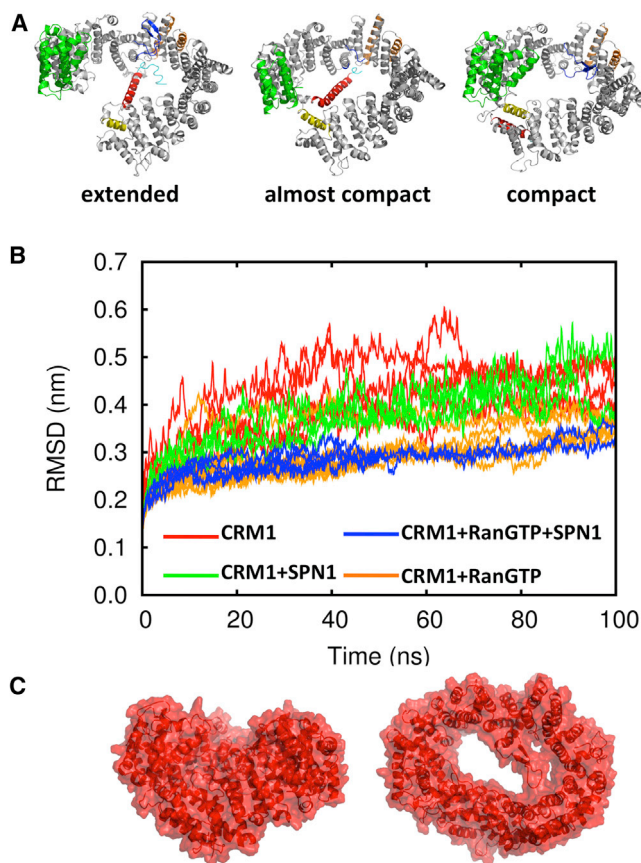
Figure 1. Changes of the Overall Structure of CRM1 during MD Simulations

(A) Crystal structures showing the three most prominent conformations of CRM1. Left: Extended conformation as in free CRM1 (4FGV) with no interaction between N- (green) and C-terminal regions (HEAT helix 21A, yellow); the AL (blue) in the flipped back position and the HEAT helix 21B (red) in the bridging position. The NES binding cleft is shown in orange. In the almost compact conformation as in the CRM1-SPN1 complex (3GB8), few interactions between N- and C-terminal regions are seen, the AL is not resolved, and helix 21B is in the bridging position, but exhibits a kink. In the compact conformation as in the CRM1-RanGTP-SPN1 complex (3GJX), close contacts between N- and C-terminal regions are seen, the AL is in the seatbelt conformation, and helix 21B is in the parallel position on the outside of the CRM1 molecule.

(B) Structural changes of CRM1 in the ternary complex during MD equilibration, monitored by the RMSD to the crystal structure (3GJX; blue curves). Changes in the rmsd of CRM1 in complex with either RanGTP or SPN1 are shown in orange or green, respectively; the red curves represent changes for CRM1 alone.

(C) CRM1 maintains a toroidal structure during MD simulations as shown by a snapshot of CRM1 in the free form after a 100-ns simulation (bottom right). See also Figures S1 and S2 and Tables S1 and S2 for additional information.

shape with the N- and C-terminal HEAT repeats in close contact (Koyama and Matsuura, 2010; Monecke et al., 2009). A coexisting less compact but still toroidal shape has been described during some states of its transport cycle (Dong et al., 2009b; Figure 1A). Recent structural analysis of free CRM1 from *Chaetomium thermophilum* (ctCRM1) and *Saccharomyces cerevisiae* (scCRM1) revealed that, in these organisms, CRM1 also adopts a more or less extended superhelical shape without close inter-

action of the N- and C-terminal regions (Monecke et al., 2013; Saito and Matsuura, 2013).

Crystal structures of various CRM1 complexes have provided insight into molecular details of the interactions between CRM1 and its interaction partners during the transport cycle. CRM1 cooperatively binds RanGTP and cargo in the nucleus (Paraskeva et al., 1999). In this ternary complex, RanGTP is localized within the ring of CRM1 and bound by N- and C-terminal HEAT repeats as well as the acidic loop (AL). The AL is inserted between the helices of HEAT repeat 9 (H9) and affixes the GTPase to the terminal HEAT repeats like a seatbelt (Monecke et al., 2009). Remarkably, the cargo binds on the opposite side of CRM1 without direct contacts to RanGTP. It predominantly interacts with acidic patches on the outer surface of CRM1 and a groove formed between the α helices of H11 and H12 (Dong et al., 2009a, 2009b; Monecke et al., 2009). A common motif required for binding of cargo within this groove is the leucine-rich nuclear export signal (NES) consisting of a short peptide stretch of 10–15 residues (Güttler et al., 2010). The CRM1-RanGTP-cargo complex traverses the NPC and enters the cytosol, where it dissociates upon binding of disassembly factors such as RanBP1, which function as cargo release factors and increase the hydrolysis rate of Ran-bound GTP when binding to RanGAP (Askjaer et al., 1999; Koyama and Matsuura, 2010; Maurer et al., 2001; Paraskeva et al., 1999). Free CRM1 shuttles back to the nucleus for another round of export. The reported crystal structures reveal snapshots of various states during the transport process and show the interaction surfaces of CRM1 with cargo and/or Ran. Due to the growing medical interest in CRM1 and its role in cancer (Turner et al., 2012), it is important to understand the dynamics of human CRM1 with a focus on the NES-binding cleft where many therapeutics bind. Purely static structure characterization alone is insufficient for a complete description of structural changes during the transport cycles. Recent findings from MD simulations on the free—extended—form of CRM1 from the lower eukaryote *C. thermophilum,* have shown that the α helix of H21, but not the AL, contribute significantly to the ratio between the extended and the compact form of CRM1 (Monecke et al., 2013). In the ternary complex of CRM1-RanGTP-SPN1, the altered arrangement of the AL, bridging the central opening and linking two distant regions of CRM1, suggests a structural role for determining both the overall conformation of CRM1 and that of the NES-binding cleft. Moreover, the role of RanGTP in restricting the conformational flexibility of CRM1, especially regarding the NES-binding cleft, and the opening mechanism of the toroidal form of CRM1 toward the extended conformation are still open questions. Here, small-angle X-ray scattering (SAXS), electron microscopy (EM), and molecular dynamics (MD) simulations were combined with the available information from crystal structures to elucidate the structural transitions and forces required for the cooperative binding and release of RanGTP and/or the cargo Snurportin1 (SPN1) to mammalian CRM1. We find that mammalian CRM1 in the free form reveals a high degree of conformational flexibility. Binding of RanGTP decreases this flexibility and shifts the conformation toward a more rigid, compact form of CRM1. Our results also show that the AL has a strong influence over the state of the NES-binding cleft. We conclude that RanGTP binding in the presence of the AL ensures

Table 1. Characteristics Determined by SAXS Measurements

	R_g (nm)	D_{max} (nm)	Porod (nm^3)	Estimated Molecular Mass (Porod)	Expected Molecular Weight
mmCRM1	3.8 ± 0.1	11 ± 1	190 ± 20	120 ± 10	121
hsCRM1	3.9 ± 0.1	11 ± 1	180 ± 20	110 ± 10	121
hsCRM1 + SPN1	4.1 ± 0.4	14 ± 1	260 ± 20	160 ± 15	162
mmCRM1 + RanGTP (+NES)	3.6 ± 0.1	10 ± 1	230 ± 20	140 ± 15	141
mmCRM1 + RanGTP + SPN1	4.1 ± 0.1	14 ± 1	300 ± 30	190 ± 20	183

All data were calculated using the programs indicated in the Supplemental Experimental Procedures.
See also Tables S1 and S2.

that the NES-binding cleft for export cargo remains in an open conformation prone for NES binding, and thus enhances the affinity for cargo.

RESULTS AND DISCUSSION

Free MD Simulations of Mammalian CRM1

To gain insight into the atomic rearrangements in mammalian CRM1 during disassembly, we performed multiple unrestrained 100-ns MD simulations of the mouse (mm)CRM1-RanGTP-SPN1 ternary complex (Protein Data Bank [PDB] ID: 3GJX) and on the same assembly structure after removing either SPN1 or/and RanGTP. Global conformational changes were monitored by calculation of the Cα root-mean-square deviation (rmsd) values relative to the crystal structure (Figure 1B). The ternary complex in solution shows a significant increase in the backbone rmsd of CRM1 only in the first 2–5 ns (Figure 1B). This probably reflects a fast adaptation or relaxation from a polyethylene glycol (PEG)-containing condition, in which the crystals were grown, to a PEG-free solution in the MD simulation. Moreover, we considered individual complexes in the simulations, relieving possible strain from crystal contacts. After this initial phase, only a moderate increase of the rmsd is seen during the rest of the simulation. When SPN1 was removed, CRM1 underwent only little additional overall change (Figure 1B), as indicated by the small rmsd increase. The conformational stability of the CRM1-RanGTP-SPN1 and CRM1-RanGTP complexes is also reflected by the radius of gyration of CRM1 (R_g), which remains stable during the simulations (Figure S1 available online).

The overall rmsd of free CRM1 is increased over the ternary complex and stronger fluctuations in R_g are observed (Figures 1B and S1A). The CRM1-SPN1 complex exhibited an intermediate rmsd behavior, increasing more markedly than that of the CRM1-RanGTP-SPN1 complex and reaching the values of free CRM1 at the end (Figure 1B). Overall, the shape of CRM1 stayed ring-like in all simulations (Figure 1C), and the AL remained near the seatbelt conformation observed in the crystal structure (Figures S1B and S2). In all cases, after 100 ns of simulation, the overall rmsd had still not fully converged, indicating that the simulations had not yet reached equilibrium and that further structural rearrangements may take place on a larger timescale.

In contrast to the simulations, the structures of free CRM1 from *C. thermophilum* (4FGV and 4HZK; Monecke et al., 2013) and *S. cerevisiae* (3VYC; Saito and Matsuura, 2013) show CRM1 to adopt a more or less extended superhelical shape, respectively. Because these conformations are not observed in

the MD simulations, the question arises whether the extended conformations are specific to CRM1 from lower eukaryotes or if such a conformational change is inaccessible on the time scale of MD simulations. To clarify this question, we performed EM and SAXS experiments to elucidate the global shape and the extent of rearrangement of the AL in mammalian CRM1.

SAXS Measurement, Ab Initio Modeling and Subtractive Modeling of Mammalian CRM1 and Complexes

Human (hs)RanGTP, hsSPN1, hsCRM1, and mmCRM1 (differing only in a few residues; Figure S3) were purified, and the individual complexes were assembled and then analyzed. CRM1 in complex with only RanGTP could not be analyzed due to instability of the complex (Dong et al., 2009b). Thus the complex of CRM1 and RanGTP was stabilized by a short peptide resembling a leucine-rich NES. The SAXS of CRM1, the ternary complexes of CRM1-RanGTP-SPN1 or CRM1-RanGTP-NES as well as CRM1 in complex with SPN1 were measured, and the data were processed, merged, and analyzed (Figure S4A). The Porod volumes and corresponding molecular masses for all samples are consistent with monomeric assemblies in solution (Table 1). The maximum sizes D_{max} and the R_g values (Table 1) were calculated from the distance distribution functions. With use of the range of scattering vectors up to s = 0.2 Å^{-1}, low resolution ab initio models of CRM1 alone and of the complexes were constructed (Figures 2 and S4). The ab initio reconstruction from the free CRM1 data yielded a toroidal structure (discrepancy χ = 1.7; Figure 2A). Theoretical scattering patterns of free CRM1 in the extended form (4FGV) and in the compact form, extracted from the ternary complex (3GJX), were computed (see Experimental Procedures). The calculated curves differ significantly from the experimental SAXS results (Figure S5A) so that neither the extended nor the compact form (χ = 3.2 and χ = 3.4, respectively) fit well. Better fits were obtained using free ctCRM1 (4HZK) and scCRM1 (3VYC), which are less extended than CRM1 in PDB ID 4FGV, and with hsCRM1 extracted from PDB ID 3GB8. The better fit for the latter is in agreement with recent results (Fox et al., 2011), but one should note that in all these structures, up to 12% of atoms present in full CRM1 are not resolved (see legend of Table S2).

The CRM1-SPN1 complex reveals a toroidal shape of CRM1 with SPN1 attached on the outside (Figure 2C). The theoretical scattering curve computed from the binary complex extracted from 3GJX shows a significant misfit to the experimental data (χ = 2.8). The conformation in solution revealed by SAXS appears therefore noticeably more extended than the structure observed
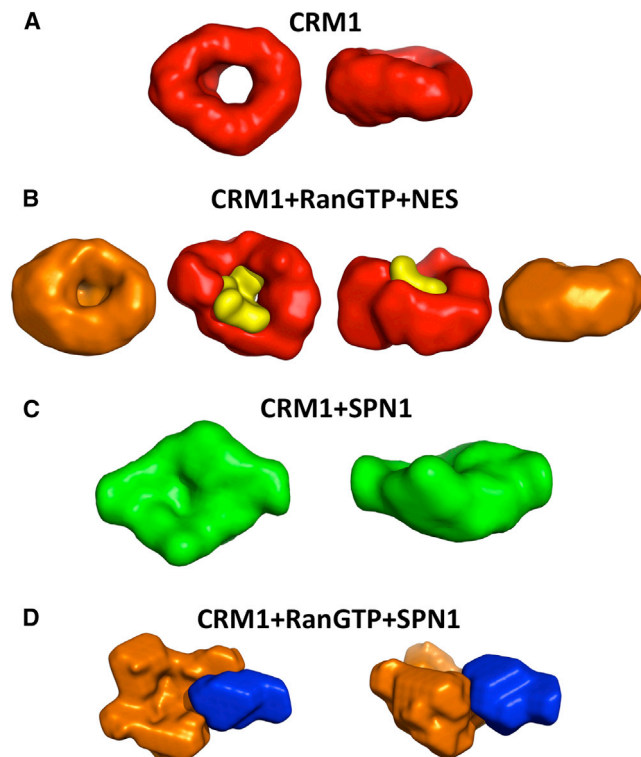
Figure 2. Localization of the Individual Components of the CRM1 Complexes by Comparative Structure Determination Using the Set of SAXS Data Curves

Processed solution scattering patterns from mmCRM1, mmCRM1-hsRanGTP, hsCRM1-hsSPN1, and mmCRM1-hsRanGTP-hsSPN1 (Figures S3–S5) were used to calculate the ab initio models.

(A and B) CRM1 depicted in red (top) reveals a toroidal shape in solution (A) and maintains this shape upon RanGTP binding (B, orange model). Modeling of the individual molecules localizes RanGTP (yellow) in the hollow of CRM1 (red).

(C) SPN1 bound to CRM1 (green model).

(D) SPN1 (blue) clearly localizes to the outer surface of CRM1 (CRM1 and RanGTP in orange).

See also Tables S1 and S2.

in the ternary complex and, given that the domains of SPN1 itself are expected to be rather rigid (Table S1), this points to an extended structure of CRM1 itself. The extended conformation more likely resembles the one observed in the CRM1-SPN1 structure (3GB8).

For CRM1 in complex with RanGTP and NES (Figure 2B) or, RanGTP and SPN1 (Figure 2D), the ab initio models show Ran positioned in the central opening seen for free CRM1. Interestingly, both R_g and D_{max} of CRM1 alone are larger than those for CRM1 in complex with RanGTP, again indicating that CRM1 changes its structure and adopts a more compact conformation upon binding RanGTP. The average R_g values obtained by SAXS are in good agreement with the R_g values for snapshots from the individual MD simulations and the X-ray structures (Table S2).

The overall shape of CRM1 is still recognizable in the ab initio reconstruction derived from the curve of the CRM1-RanGTP-NES complex, but the complex seems to adopt a more compact form. An additional part is observed located close to one side of

the ring and to the central opening (discrepancy $\chi = 2.0$; Figure S4C). By simultaneously fitting the experimental curves of the different samples, multiphase ab initio models were built (see Supplemental Experimental Procedures) to gather information of the relative orientation and position of the individual proteins within the complexes. The models fit the experimental data quite well, with a discrepancy of $\chi = 1.2$ for the curve of CRM1 alone and $\chi = 1.2$ for CRM1-RanGTP-NES. The result for the CRM1-RanGTP-NES complex clearly shows CRM1 as a torus with RanGTP in the central opening (Figure 2B). This result is in good agreement with the crystal structure of the CRM1-RanGTP complex (3NC1).

The ab initio structure reconstructed from the SAXS pattern of CRM1-RanGTP-SPN1 clearly adds volume to the outer surface of the CRM1 ring thus localizing SPN1 exactly at this position (discrepancy $\chi = 1.8$; Figures 2D). Due to the fact that the curves obtained for CRM1 alone and in complex with RanGTP differ in R_g and D_{max}, the position of SPN1 in the ternary complex can be determined only with regard to the CRM1-RanGTP complex. In the resulting model (fitting the data with $\chi = 1.3$), SPN1 appears as an appendix attached to the outside of the CRM1-RanGTP-NES shape (Figure 2C).

Taken together, the SAXS data strongly indicate that unbound mammalian CRM1 exists in a more extended structure in the measured ensemble of molecules and that binding of RanGTP and NES peptide and/or SPN1 reduces the shape to a more compact conformation.

Single Particle EM Structures of Human CRM1 in the Free Form

We next addressed the question whether the different conformations of free hsCRM1 can also be seen on a single molecule level in a noncrystalline environment. For this purpose, hsCRM1 was subjected to the GraFix approach—a method allowing the stabilization of different structural populations that exist in solution—and subsequent single-particle EM analysis (Figures S6 and S7). As expected, the human sample showed much higher flexibility when fixed at 4°C compared to our previous study on the *C. thermophilum* CRM1 (Monecke et al., 2013). Thus, to reduce the number of conformations, this stabilization was performed at −10°C. As also seen for ctCRM1, free hsCRM1 occurs in two different and clearly distinct conformations. However, while approximately two thirds of ctCRM1 adopt an extended and pitched superhelical conformation, about half of the human particles (19,254 of 42,108) classified to this shape (Figure 3), similar to that seen in the crystal structure of free ctCRM1. The other conformer, represented by the remaining half of the particles, resembles the shape of a distorted toroid, reminiscent of the CRM1 conformation observed in various binary and ternary complexes. Interestingly, in contrast to the *C. thermophilum* homolog, resampling methods allowed us to predict a large number of subpopulations for the compact conformer, which could not be separated further (Figure S7).

The observation of the high conformational flexibility of free hsCRM1 in the EM prompted us to reinvestigate the results of free CRM1 obtained by SAXS. As mentioned previously, neither the extended nor the compact form of CRM1 fit the SAXS data well. Moreover, the R_g determined experimentally lies within the range between the calculated R_g of the extended and

extended (4FGV)

Compact
superposed with

3GB8   **3GJX**
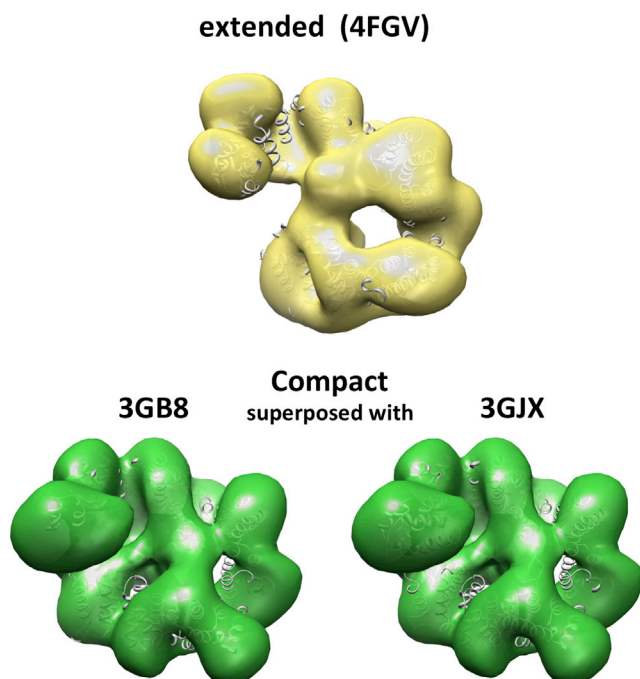
Figure 3. Electron Microscopy Analysis of Free *Homo sapiens* CRM1

EM models of the compact (green) and the extended conformation (yellow) of free *hs*CRM1 (see also Figures S6 and S7). The crystal structures of free *ct*CRM1 (4FGV) and CRM1 derived from the complex structures with SPN1 (3GB8) or the ternary complex with RanGTP and SPN1 (3GJX) are fitted to the envelope models of the EM structures as indicated.

See also Table S3.

compact conformations of CRM1, suggesting a mixture of these two conformations. The best fit for the experimental data of free CRM1 from human and mouse could therefore be obtained with a mixed population using a ratio of roughly 40:60 between extended and compact structures of CRM1 (4FGV/3GJX; Table S3). Please note that only these crystal structures were used because they include 98% of all atoms.

Taken together, the EM results show that free CRM1 in solution exists in open extended, superhelical conformations alongside the compact circular conformations. Whether the observed compact conformations are fully compact as in the ternary complex structure or represent the almost compact conformations as seen for the CRM1-SPN1 complex, cannot be answered unambiguously. The fact that no extended structure was observed in the 100-ns MD simulations indicates that the different conformations are separated by considerable energy barriers.

### MD Simulation: Toward an Open CRM1 Structure

To better understand the nature of the forces that oppose the opening of the compact CRM1 and the increase of the superhelical pitch, we focused on two sites of interest both residing within CRM1, i.e., the AL and the contact site between the N- and C-terminal regions, including the C-terminal helix 21B (Dong et al., 2009b; Koyama and Matsuura, 2010; Monecke et al., 2009). The crystal structures suggest that, on one hand, the AL tends to stabilize a compact CRM1 conformation when

engulfing Ran (Figure 1A). This conformation is rearranged when RanBP1 is bound (as in 3M1I) toward a "flipped back" conformation, and remains in this state in the more extended conformations (as in 4FGV, 4HZK, and 3VYC). Helix 21B, on the other hand, adopts two different conformations in the available crystal structures. In the compact form, it is arranged in the HEAT repeat-like "parallel" fashion and located at the outside of CRM1 (3GJX). In contrast, in the other conformations it spans the central opening of CRM1 ("bridging"), contacting residues in the region forming the NES-binding cleft (3GB8, 4FGV, 4HZK, and 3VYC; Figure 1A). The major differences between the extended form and an observed intermediate, the almost compact conformation, are the number of contacts between the N- and C-terminal regions and the fact that the C-terminal acidic patch is in contact with the HEAT repeats that line the NES-binding cleft only in the extended conformation.

As a first step, the role of the N- and C-terminal interactions in maintaining a toroidal conformation was investigated in the presence and absence of the AL. In force-probe MD simulations, both the N- and C-terminal regions of CRM1 were subjected to pulling potentials acting in opposite directions. The forces were applied close to the interface where the N- and C-terminal regions contact each other to form a toroid or closed solenoid (Figure S8A). In most simulations, the force led to rupture of the ring-closing contacts without severely perturbing the HEAT repeats (Figure 4A). All simulations resulted in extended, super-helical structures with a high flexibility and a varying degree of pitch within less than 1 ns. These global conformations are quite similar to the open conformations of superhelical KAPs, such as the prototypic solenoid Impβ. Rupture of the toroid interface is associated with a peak in the force curves (Figure 4A), seen here at 0.4 ns simulation time. To test whether enforced opening of CRM1 is reversible, we performed relaxation simulations, allowing the extended conformational states of CRM1 to evolve freely (Figure 4C). Indeed, within 10 ns, CRM1 recovered a ring structure after release of the pulling force, as indicated by a decrease of both R_g and the rmsd relative to the compact conformation (Figure 4B). An overlay of the recovered conformation with the initial CRM1 ring shows their high structural similarity (Figure 4C). A notable exception is the exact pattern of close contacts at the interface between the N- and C-terminal regions.

In summary, these simulations show that CRM1 can be brought into an elongated, superhelical conformation similar to Impβ when the contact between the N- and C-terminal regions is ruptured by external mechanical strain. The extended conformation of CRM1 shows the major hallmarks of an α solenoid, i.e., high overall flexibility under simultaneous stability of the secondary structure elements. The remarkably high transition rates observed for returning to its original equilibrium conformation are similar to those seen for the global conformational changes of Impβ (Kappel et al., 2010). They thus appear to be a general feature of nuclear transport receptors.

To further characterize the driving forces for connecting the N- and C-terminal regions and for stabilizing the connection, we tested whether the mechanical properties of CRM1 after a cycle of pulling and relaxation are similar to those of the initial structure. Stretching simulations were repeated on relaxed CRM1 structures with pulling potentials acting on the terminal sections.
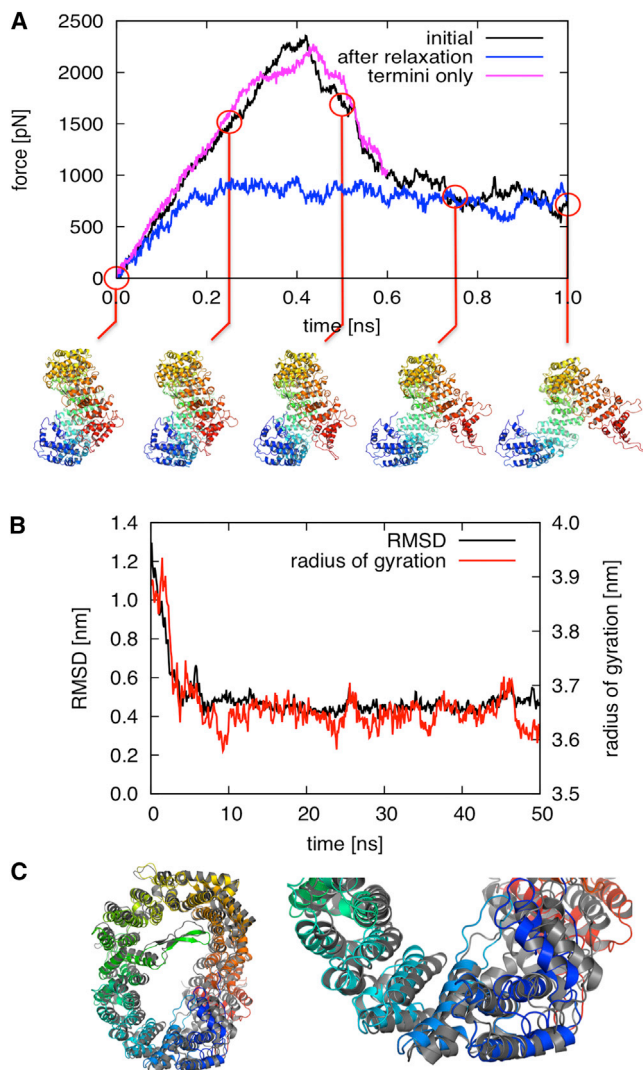
Figure 4. CRM1 Stretching and Relaxation

(A) Force profiles obtained from simulations with a probe velocity of v = 5 m/s: initial stretching (black), stretching after relaxation (blue), and stretching of a structure containing only the terminal regions (magenta). The red circles denote the times the snapshots shown below were taken. Colors are in rainbow progressing from N terminus (blue) to C terminus (red).

(B) Backbone rmsd with respect to the initial structure (solid black lines) and R_g (solid red line) of CRM1 during relaxation.

(C) The left panel shows an overlay of the initial CRM1 structure (gray) and a structure after 50 ns of relaxation. The right panel shows a close-up of the region connecting the termini. Structure and colors as in (B).

See Figure S8 for experimental setup and additional information.

In contrast to the initial simulations, repeated stretching did no longer lead to pronounced force peaks, i.e., a much lower force was now required to separate the terminal regions of relaxed CRM1 (Figure 4A). This lack of interaction forces might either be due to a perturbation of the global elastic properties of CRM1 caused by the opening/closing cycle, i.e., a change in the microscopic interaction pattern within and between all HEAT repeats, or, alternatively, to the loss of important interactions at the interface between the terminal regions.

To differentiate between these two possibilities, additional force probe simulations with only N- and C-terminal fragments of CRM1 were conducted (residues A12–V274 and I815–S1055, in the absence of in-lying HEAT repeats; Figure S8B). The observed force peaks and required force for separating the terminal fragments is nearly identical to that needed to rupture these contacts in full CRM1 (Figure 4A). This suggests that the main contribution to ring closure comes from the interfacial contacts between the N- and C-terminal regions rather than from strain within the body of CRM1. Indeed, because the forces needed to rupture the terminal interface are larger than those seen for stretching the protein, the terminal interactions might even serve to maintain mechanical strain and, thereby, store energy within the array of HEAT repeats. Overall, the force probe simulations suggest that the arrangement of HEAT repeats is compatible with both extended and compact conformations of the free CRM1. The latter is stabilized by specific interactions between the terminal regions. After stretching and release, these contacts are not fully recovered during the simulations, probably due to the presence of many local minima, separated by high energy barriers.
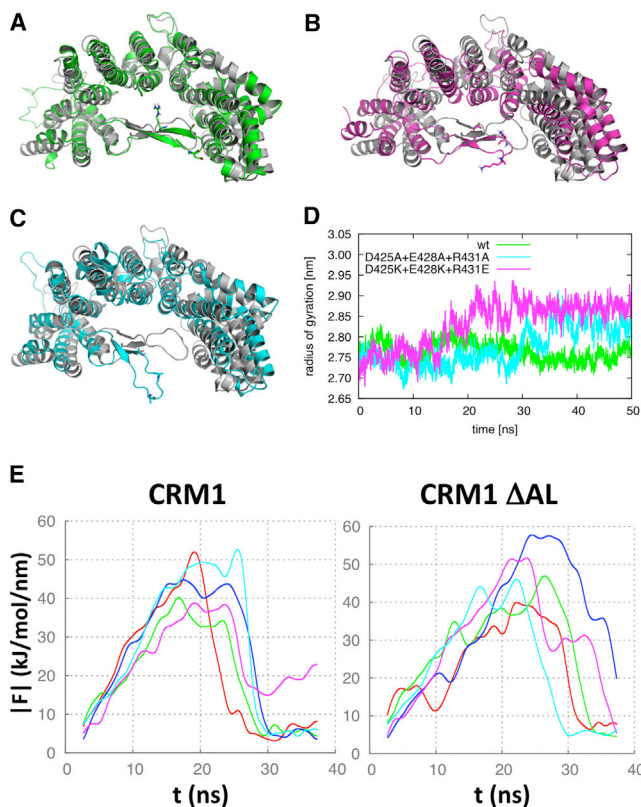
In contrast to other KAPs, the AL in CRM1 is markedly longer and forms a more rigid structural element consisting of a long β-hairpin. It links the two α helices of H9 and affixes RanGTP to CRM1 like a seatbelt, contacting H12–H15 opposite H9. The observed local rigidity in that region is an intrinsic property of CRM1. We next analyzed whether it directly arises from interactions of the AL by performing simulations on a fragment of CRM1 comprising only the central HEAT repeats including the AL (residues R344–L811; Figure S8B). The structure of this fragment remained stable for 50 ns, as shown by its R_g and structural snapshots (Figures 5A and 5D). Closer analysis revealed that three residues within the AL (D436, E439, and R442) form particularly strong electrostatic interactions to the α helices of H12, H14, and H15. Their role in rigidifying the central CRM1 section was therefore examined further. In simulations of CRM1 charge reversal mutants (triple mutation D436K/E439K/R442E, Figure 5B), in which the interactions of the AL with the opposing face of the CRM1 ring are abolished, the central region showed a significant change in its curvature within 50 ns (Figure 5D). Further simulations, in which these residues were each mutated to alanine, displayed a similar change in shape (Figures 5C and 5D).

In summary, the conformation of CRM1 is regulated by a complex pattern of interactions between successive HEAT repeats, the interface between the terminal regions, the AL, and the C-terminal helix 21B.

MD Analysis of Structural Changes in Ran and NES Binding Sites

Two prominent mechanisms are conceivable to explain how the AL mediates cooperative binding of RanGTP and SPN1. One idea is that the AL in the seatbelt conformation may stabilize the compact conformation, which then shifts the equilibrium at the NES-binding cleft toward a conformation prone for cargo binding. Alternatively, the conformation of the AL might directly determine the conformational state of the NES-binding cleft, thereby coupling the global conformation to the NES-binding site. To test the first idea, we recorded the rupture force in MD

Table 2. Average Rupture Forces Calculated from Independent Force Probe Simulations for CRM1 WT or AL Deletion Mutant

| $F_{rupture}$ kJ/(mol*nm)	3GJX WT	3GJX w/o AL
Initial	45.7 ± 2.6	48.5 ± 2.7
Slower	42.6 ± 2.3	37.0 ± 2.9

The average rupture forces for the force probe simulations in the presence or absence of the AL at two velocities are shown.

Figure 5. Influence of the AL on CRM1 Conformation

(A–C) Snapshots at the start (gray) and after 50 ns (colored) of each simulation. Key residues are shown in stick and sphere representation. The panels show wt CRM1 (A, green), mutant D436K/E439K/R442E (B, magenta), and mutant D436A/E439A/R442A (C, cyan).

(D) R_g of the WT and the two mutations for each single simulation. Raw data (symbols) and Gaussian filtered data (lines) are shown. Colors as in (A)–(C).

(E) By applying a time-dependent harmonic biasing potential, CRM1 is brought from the compact into the extended conformation. The average over the maximally occurring forces during these force probe simulations, the rupture force, is related to the energetic barrier separating compact and extended conformation. Comparing these rupture forces for WT (left) and AL deletion mutant (right) simulations reveals that the AL does not significantly influence this energetic barrier (see also Table 2).

simulations with an external biasing potential that drives the compact (3GJX) structure toward the extended (4FGV) conformation, both for the wild-type (WT) and an AL deletion mutant (Figure 5E). Remarkably, no significant difference was observed between these variants, and this result was robust under variation of the pulling velocity (Table 2; Figure S8C). These findings suggest that the energy required for the compact-to-extended transition of CRM1 is dominated by the interactions between the C- and N-terminal regions, whereas the AL seems to play a rather minor role. Indeed, closer analysis of the simulations showed that the AL maintains all interactions that stabilize the seatbelt conformation even after this enforced conformational change.

Next we investigated the influence of the AL on the configuration of the NES-binding cleft by carrying out unbiased simulations of WT CRM1 and the AL deletion mutant, both in the presence and absence of RanGTP. Here, the progression of

the conformational transition of the NES-binding cleft was characterized by projecting its structure onto the difference vector between the compact and extended conformations. In most simulations with bound RanGTP and in the absence of the AL, the NES-binding cleft closed within 10–60 ns (Figure 6B). By contrast, in WT CRM1 the cleft remained open during all five 100-ns simulations (Figure 6A). This observation strongly suggests that the AL mediates the cooperative binding of RanGTP and a cargo protein by stabilizing the open configuration of the NES-binding cleft.

In the absence of RanGTP, the NES-binding cleft of WT CRM1 in the compact conformation adopts an intermediate, semi-open state (Figure 6C). For the AL deletion mutant in the compact conformation without RanGTP, the ensemble of ten trajectories is probably not fully converged, as inferred from the bimodal distribution (Figure 6D). Because several closing but no re-opening events of the NES-binding cleft are seen during the 200-ns simulations, we assume that the kinetics are slowed down, with the closed cleft conformation still favored energetically.

Taken together, these results support the hypothesis that the AL directly determines the NES-binding cleft configuration. In contrast, the AL is unlikely to play a major role in the stabilization of the compact ring-like configuration of CRM1. Our finding that the AL conformation is correlated to the arrangement of the HEAT repeats lining the NES-binding cleft leads us to suggest that RanGTP facilitates cargo uptake by fine-tuning the orientation of the central HEAT repeats and, in particular, the NES-binding cleft between helices 11A and 12A. These results also support a model in which RanBP1 disassembles the complex by causing a rearrangement of the AL (Koyama and Matsuura, 2010), which leads to a shift in the relative free energy of the binding cleft conformations. This in turn decreases the affinity for cargo, resulting in its release and subsequent closure of the NES-binding cleft. Thereby the overall compact conformation of CRM1 is destabilized, facilitating full disassembly of the complex.

To test this idea further, we investigated structural changes among the HEAT repeats upon cargo and Ran binding. These structural units have been shown to be quite rigid, so major overall structural changes predominantly rely on alterations of inter-HEAT repeat interactions (Forwood et al., 2010; Kappel et al., 2010). We monitored the movements of HEAT repeats in unbiased MD trajectories starting from the crystal structure of the ternary complex (3GJX), either complete or after removal of Ran and/or SPN1. Figure 7 shows the backbone rmsd of the 21 individual HEAT repeats. The center of mass (COM) distance of neighboring HEAT repeats is plotted in Figure S9. In all cases, the closed shape of CRM1 remained intact after a simulation time of 100 ns, as reflected by the generally low rmsd with only
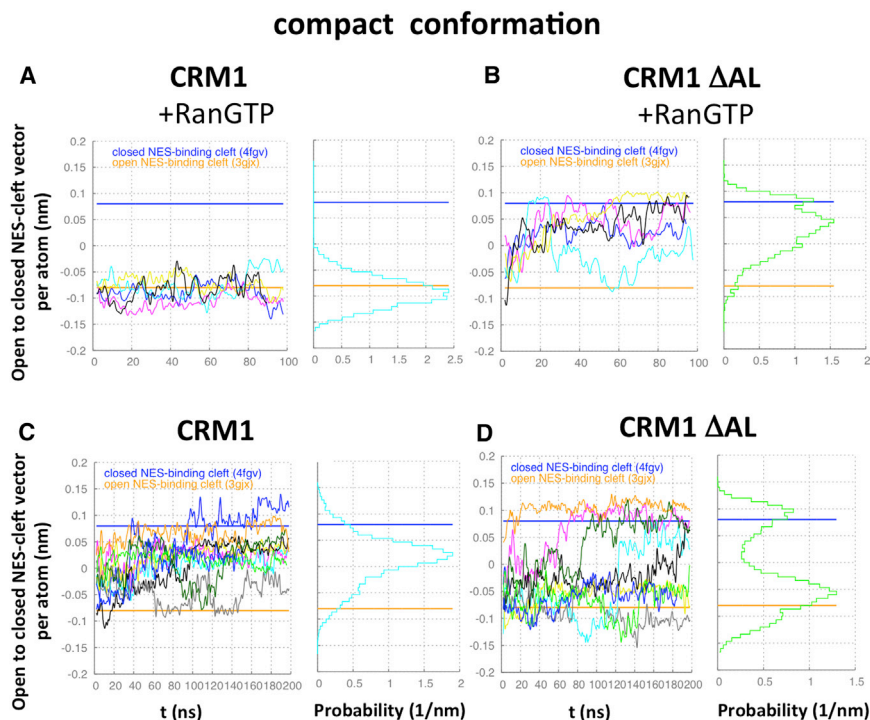
Figure 6. The AL Influences the Conformation of the NES Cleft in the Compact Toroid of CRM1

Projections of unbiased WT and AL deletion mutant simulations onto the vector connecting the open and the closed NES-binding cleft configuration, serving as a reaction coordinate to quantify open/close transitions of the NES-binding cleft. The open NES-binding cleft configuration was taken from the compact CRM1 structure (3GJX), the closed one from the extended CRM1 structure (4FGV). In (A)–(D), the vector coordinate values (per atom) for the open and closed reference structures are shown as horizontal lines. The histograms on the right are constructed from the data of all shown simulations.

(A) In WT simulations and under presence of RanGTP, the NES-binding cleft remains open in all 100-ns simulations.

(B) In AL deletion mutant simulations, spontaneous closure of the NES cleft is seen.

(C) In the absence of RanGTP, the NES-binding cleft adopts an intermediate conformation in WT simulations.

(D) Several closing but no reopening events of the NES-binding cleft are observed in AL deletion mutant simulations in the absence of RanGTP, indicating that the closed conformation is more stable.

the N-terminal HEAT repeats as exception. In light of the EM and X-ray results, this finding implies that either opening of CRM1 is intrinsically slower or that additional factors are required to promote this transition.

In contrast, the three N-terminal HEAT repeats revealed a high degree of flexibility and underwent marked conformational rearrangements during the 100-ns simulations (Figure 7). These HEAT repeats form the main RanGTP binding site (CRIME domain), which is the most highly conserved domain within the Impβ superfamily (Fornerod et al., 1997; Görlich et al., 1997; Petosa et al., 2004). This domain is more flexible than the other HEAT repeats, which suggests a weak binding of RanGTP as shown in biochemical assays (Paraskeva et al., 1999; Petosa et al., 2004). Even with RanGTP bound, the H1 helices show a noticeable degree of conformational fluctuations (Figures 7A and 7D). When RanGTP is removed from the complex, the flexibility of H1 increases further (Figures 7B and 7C), consistent with the CRM1-SPN1 crystal structure.

While changes in flexibility and conformation of the N-terminal region of CRM1 upon RanGTP-binding are clearly reflected in the rmsd, the regions involved in cargo binding seem unaffected by the presence of the binding partners. In the case of SPN1, the binding site is composed of three patches: the NES-binding cleft formed by the outward-oriented α helices of H11 and H12, the intra HEAT loop regions of H12–H14, involved in the interaction with the cap-binding domain, and the binding site for the SPN1 C-terminal region, formed by the α helices of H14–H16. Because the NES-binding cleft is the most important of these patches, the putative changes in H11 and H12 were monitored by recording their COM distance in the simulations (Figure 8A). When an NES is bound in the cleft, the distance remains at 1.7 nm (Figures 8B and S10E), as expected from the X-ray structure (3GJX). This

value agrees well with other cargo-bound CRM1 structures (1.59–1.64 nm distance; 3GJX, 3NC0, 3NBY, 3NBZ, and 3GB8; Figure S11). Removal of both RanGTP and SPN1 from the starting model results in a fast decrease of the distance between H11 and H12, indicating a closure of the NES-binding cleft toward a conformation incompatible with NES binding (Figures 8B and S10A). In free CRM1, the distance decreases for all trajectories from 1.7 nm to less than 1.5 nm and as low as 1.3 nm. In all cases, this conformation was attained within the first 50 ns and thereafter remained "closed" (Figure 8B). This finding is in agreement with previous simulations of free ctCRM1 in the extended conformation (Monecke et al., 2013), where the probability to observe the NES-binding cleft in an open conformation was consistently below 20%. When only the NES-bearing cargo, here SPN1, was removed from the complex with RanGTP still bound, larger distance fluctuations were seen; however, in four of five trajectories, the average distance remained within 0.1 nm of those obtained for the ternary complex, and similar to the respective X-ray structure (1.64 nm; 3NC1). The fifth trajectory eventually approached a more closed conformation (Figure S10B and S10C). In contrast, the AL remained in the original seatbelt conformation in all simulations (Figure S1B). We conclude that, although RanGTP is not in direct contact with H11 and H12, RanGTP binding markedly shifts the equilibrium from a closed conformation of the NES-binding cleft toward an open one, capable of binding cargo.

Interestingly, in the X-ray structures of CRM1-RanGTP-RanBP1, the AL is found in a "flipped back" configuration, which might prevent more pronounced changes in the conformation of the NES-binding cleft. In one of the structures, the NES-binding cleft is empty, which is probably why, previously, this AL arrangement was assumed to displace the cargo from the NES-binding cleft and prevent cargo rebinding (3M1I; Koyama
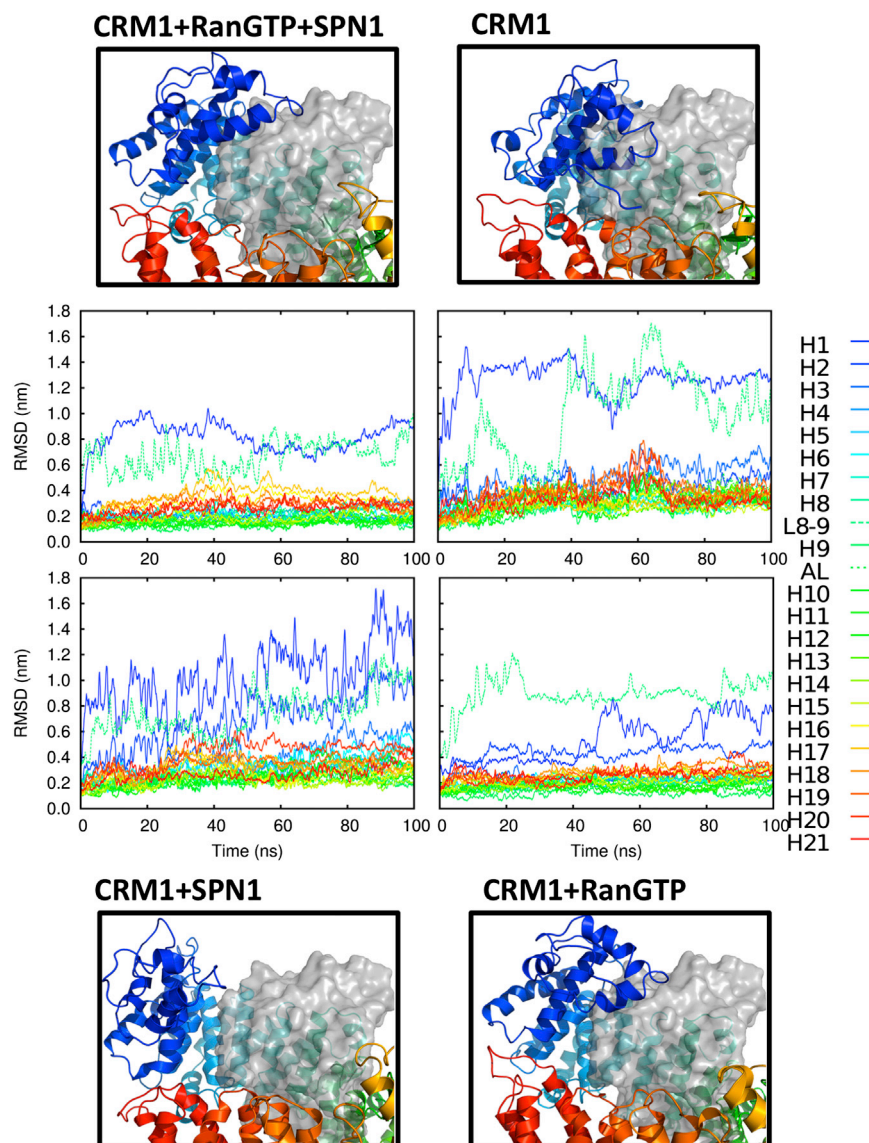
Figure 7. Significant Structural Rearrangements in CRM1 Related to the Respective Binding Partners Are Predominantly Observed within the N-Terminal HEAT Repeats
The spatial changes (C rmsd) of the 21 individual HEAT repeats are plotted over time with CRM1 from the crystal structure 3GJX as reference. The individual HEAT-repeats and relevant loops are labeled according to the color code shown on the right. The most prominent changes within the simulations are observed in the three N-terminal HEAT repeats (see also Figure S9). The respective structures are presented: CRM1-RanGTP-SPN1, CRM1, CRM1-SPN1, and CRM1-RanGTP.

Taken together, the MD simulations show that even in the compact toroidal conformation of CRM1, RanGTP binding markedly shifts the equilibrium toward the open conformation of the NES-binding cleft, thus favoring NES binding.
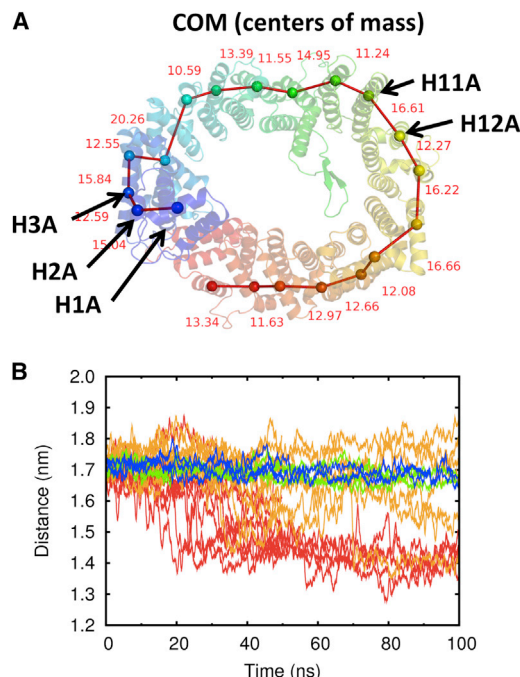
Conclusions

By combining X-ray crystallography, SAXS, single particle-EM, and atomic simulations, we showed that free human and mouse CRM1 are both highly flexible molecules. Free CRM1 can adopt multiple conformations as shown by electron microscopy and indicated by SAXS, ranging from extended conformations without interactions between N- and C-terminal regions to almost compact ones. In ternary complexes, CRM1 is in a compact toroidal conformation, corresponding to that in the known crystal structures of export complexes. Our experimental data extend earlier studies on ctCRM1 and scCRM1 to higher eukaryotes, and show that structural rearrangements are a general property of CRM1.

Our MD simulations confirm the high flexibility of CRM1 and show that CRM1 can reversibly switch from compact to extended conformations without disrupting the array of HEAT repeats. The toroidal shape of CRM1 is mainly stabilized by strong interactions between the N- and C-terminal regions. The exact compact state conformation of CRM1 is determined by an unexpectedly complex interplay of several structural features and their mutual interactions, such as the arrangement of the HEAT repeats, conformation of the AL, and positions of the C-terminal helix 21B and C-terminal acidic patch.

Our simulations strongly suggest that RanGTP binding favors the compact conformation of CRM1. The AL is the internal CRM1 key mediator transmitting the effect of this global conformational change to the NES-binding cleft. These changes shift the equilibrium of the NES-binding cleft from a closed conformation, which is incapable of substrate binding, toward open binding-competent states, thus enabling cooperative binding of both, RanGTP and cargo. These changes also seem

and Matsuura, 2010). Recently, two additional crystal structures of this complex with small inhibitors of nuclear export bound in the NES-binding cleft have been determined (4GPT and 4GMX; Etchin et al., 2013; Lapalombella et al., 2012). All three structures display H11–H12 distances between 1.44 and 1.60 nm, similar to those obtained from our MD simulations. This finding indicates, that despite the binding of RanGTP and RanBP1 and the resulting rearrangements in the HEAT repeats around the NES-binding cleft, the cleft is still flexible enough to accommodate "cargo". In contrast, the three recently published extended conformations of CRM1 exhibit H11A–H12A COM distances between 1.31 and 1.39 nm (4FGV, 4HZK, and 3VYC). Strikingly, the width of the NES-binding cleft increases from the most extended conformation of CRM1 (4FGV) to the least extended one (3VYC). This is in good agreement with the finding that the populations of the NES-binding cleft conformations are closely coupled to the extension of the overall CRM1 structure (Monecke et al., 2013) and could resemble states more or less prone for cargo binding.

A

COM (centers of mass)

B

Figure 8. The NES-Binding Cleft Is Stabilized in an Open Conformation by RanGTP

(A) The COM of the α helices of the individual HEAT (colored spheres) repeats were calculated and their distances to neighboring HEATs monitored. Helices referred to in the text are labeled and indicated by arrows.

(B) Time evolution of the COM distance between helices 11A and 12A for the simulations of the ternary complex (blue), CRM1-RanGTP (orange), CRM1-SPN1 (green), and CRM1 alone (red; for snapshots, see Figure S10 and for correlation to known X-ray structures, see Figure S11).

to reduce the free energy barriers that separate the open from the closed state. In this way, binding of RanGTP and cargo protein at two binding sites, separated by a remarkable distance, is coupled both in terms of binding free energies and kinetics, which rationalizes the observed cooperativity in structural terms.

EXPERIMENTAL PROCEDURES

Expression and Purification

CRM1 from *Mus musculus*, RanQ69LGTP 1–180 (referred to as RanGTP in the text) as well as Snurportin1 both from *Homo sapiens* were expressed and purified as described (Monecke et al., 2009). The CRM1-RanGTP-SPN1 complex as well as the CRM1-RanGTP-PKI-NES complex were assembled and purified as described (Güttler et al., 2010; Monecke et al., 2009). Human His₆-CRM1 was expressed in *Escherichia coli* TG1 as described previously (Guan et al., 2000) and purified as described in detail in the Supplemental Experimental Procedures.

Molecular Dynamics Simulations

MD simulations comparing WT and an AL deletion mutant were carried out using GROMACS 4.5 (Hess et al., 2008; Van Der Spoel et al., 2005) with the Amber99sb force field (Hornak et al., 2006) and the SPC/E water model (Berendsen et al., 1987). All other MD simulations were carried out with the GROMACS 4 program package (Van Der Spoel et al., 2005), using the OPLS-AA force field (Friesner et al., 2001; Jorgensen et al., 1996) and the TIP4P water model (Jorgensen et al., 1983). All simulation systems were based on CRM1 as observed in the ternary complex (3GJX).

Small-Angle X-Ray Scattering

The scattering data from solutions of CRM1 alone and in complex were collected on the X33 beamline (EMBL, DORIS III, Hamburg; Blanchet et al., 2012). The data were processed by standard procedures using PRIMUS and Gnom (Svergun, 1992). The low-resolution ab initio shapes were generated using multiple runs of DAMMIF (Franke and Svergun, 2009) averaged by DAMAVER (Volkov and Svergun, 2003) and SUPCOMB (Svergun and Kozin, 2001). A multiphase shape modeling program MONSA (Svergun, 1999) was used for the low-resolution shape analysis of CRM1 in complex. The scattering from the high-resolution models was calculated with CRYSOL (Svergun et al., 1995).

Electron Microscopy Preparation and Image Processing

Purified human CRM1 was prepared and analyzed as described in (Monecke et al., 2013) with the difference that GraFix was run at −10°C. Final three-dimensional models were obtained at a resolution of approximately 20 Å.

ACCESSION NUMBERS

The EMDataBank accession numbers for the structures of CRM1 reported in this paper are EMD-2274 and EMD-5564.

SUPPLEMENTAL INFORMATION

Supplemental Information includes Supplemental Experimental Procedures, eleven figures, and three tables and can be found with this article online at http://dx.doi.org/10.1016/j.str.2013.05.015.

REFERENCES

Askjaer, P., Bachi, A., Wilm, M., Bischoff, F.R., Weeks, D.L., Ogniewski, V., Ohno, M., Niehrs, C., Kjems, J., Mattaj, I.W., and Fornerod, M. (1999). RanGTP-regulated interactions of CRM1 with nucleoporins and a shuttling DEAD-box helicase. Mol. Cell. Biol. *19*, 6276–6285.

Berendsen, H.J.C., Grigera, J.R., and Straatsma, T.P. (1987). The missing term in effective pair potentials. J. Phys. Chem. *91*, 6269–6271.

Blanchet, C.E., Zozulya, A.V., Kikhney, A.G., Franke, D., Konarev, P.V., Shang, W., Klaering, R., Robrahn, B., Hermes, C., Cipriani, F., et al. (2012). Instrumental setup for high-throughput small- and wide-angle solution scattering at the X33 beamline of EMBL Hamburg. J. Appl. Cryst. *45*, 489–495.

Chook, Y.M., and Süel, K.E. (2011). Nuclear import by karyopherin-βs: recognition and inhibition. Biochim. Biophys. Acta *1813*, 1593–1606.

Cook, A.G., and Conti, E. (2010). Nuclear export complexes in the frame. Curr. Opin. Struct. Biol. *20*, 247–252.

Cook, A., Fernandez, E., Lindner, D., Ebert, J., Schlenstedt, G., and Conti, E. (2005). The structure of the nuclear export receptor Cse1 in its cytosolic state reveals a closed conformation incompatible with cargo binding. Mol. Cell *18*, 355–367.

Cook, A.G., Fukuhara, N., Jinek, M., and Conti, E. (2009). Structures of the tRNA export factor in the nuclear and cytosolic states. Nature *461*, 60–65.

Dong, X., Biswas, A., and Chook, Y.M. (2009a). Structural basis for assembly and disassembly of the CRM1 nuclear export complex. Nat. Struct. Mol. Biol. *16*, 558–560.

Dong, X., Biswas, A., Süel, K.E., Jackson, L.K., Martinez, R., Gu, H., and Chook, Y.M. (2009b). Structural basis for leucine-rich nuclear export signal recognition by CRM1. Nature *458*, 1136–1141.

Etchin, J., Sun, Q., Kentsis, A., Farmer, A., Zhang, Z.C., Sanda, T., Mansour, M.R., Barcelo, C., McCauley, D., Kauffman, M., et al. (2013). Antileukemic activity of nuclear export inhibitors that spare normal hematopoietic cells. Leukemia *27*, 66–74.

Fontes, M.R., Teh, T., and Kobe, B. (2000). Structural basis of recognition of monopartite and bipartite nuclear localization sequences by mammalian importin-alpha. J. Mol. Biol. *297*, 1183–1194.

Fornerod, M., van Deursen, J., van Baal, S., Reynolds, A., Davis, D., Murti, K.G., Fransen, J., and Grosveld, G. (1997). The human homologue of yeast CRM1 is in a dynamic subcomplex with CAN/Nup214 and a novel nuclear pore component Nup88. EMBO J. *16*, 807–816.

Forwood, J.K., Lange, A., Zachariae, U., Marfori, M., Preast, C., Grubmüller, H., Stewart, M., Corbett, A.H., and Kobe, B. (2010). Quantitative structural analysis of importin-β flexibility: paradigm for solenoid protein structures. Structure *18*, 1171–1183.

Fox, A.M., Ciziene, D., McLaughlin, S.H., and Stewart, M. (2011). Electrostatic interactions involving the extreme C terminus of nuclear export factor CRM1 modulate its affinity for cargo. J. Biol. Chem. *286*, 29325–29335.

Franke, D., and Svergun, D.I. (2009). DAMMIF, a program for rapid ab-initio shape determination in small-angle scattering. J. Appl. Crystallogr. *42*, 342–346.

Friesner, R.A., Kaminski, G.A., Tirado-Rives, J., and Jorgensen, W.L. (2001). Evaluation and reparametrization of the OPLS-AA force field for proteins via comparison with accurate quantum chemical calculations on peptides. J. Phys. Chem. B *105*, 6474–6487.

Görlich, D., Dabrowski, M., Bischoff, F.R., Kutay, U., Bork, P., Hartmann, E., Prehn, S., and Izaurralde, E. (1997). A novel class of RanGTP binding proteins. J. Cell Biol. *138*, 65–80.

Guan, T., Kehlenbach, R.H., Schirmer, E.C., Kehlenbach, A., Fan, F., Clurman, B.E., Arnheim, N., and Gerace, L. (2000). Nup50, a nucleoplasmically oriented nucleoporin with a role in nuclear protein export. Mol. Cell. Biol. *20*, 5619–5630.

Güttler, T., Madl, T., Neumann, P., Deichsel, D., Corsini, L., Monecke, T., Ficner, R., Sattler, M., and Görlich, D. (2010). NES consensus redefined by structures of PKI-type and Rev-type nuclear export signals bound to CRM1. Nat. Struct. Mol. Biol. *17*, 1367–1376.

Hess, B., Kutzner, C., van der Spoel, D., and Lindahl, E. (2008). GROMACS 4: Algorithms for Highly Efficient, Load-Balanced, and Scalable Molecular Simulation. J. Chem. Theory Comput. *4*, 435–447.

Hornak, V., Abel, R., Okur, A., Strockbine, B., Roitberg, A., and Simmerling, C. (2006). Comparison of multiple Amber force fields and development of improved protein backbone parameters. Proteins *65*, 712–725.

Hutten, S., and Kehlenbach, R.H. (2007). CRM1-mediated nuclear export: to the pore and beyond. Trends Cell Biol. *17*, 193–201.

Jorgensen, W.L., Chandrasekhar, J., Madura, J.D., Impey, R.W., and Klein, M.L. (1983). Comparison of simple potential functions for simulating liquid water. J. Chem. Physiol. *79*, 926–935.

Jorgensen, W.L., Maxwell, D.S., and TiradoRives, J. (1996). Development and testing of the OPLS all-atom force field on conformational energetics and properties of organic liquids. J. Am. Chem. Soc. *118*, 11225–11236.

Kappel, C., Zachariae, U., Dölker, N., and Grubmüller, H. (2010). An unusual hydrophobic core confers extreme flexibility to HEAT repeat proteins. Biophys. J. *99*, 1596–1603.

Kobe, B., Gleichmann, T., Horne, J., Jennings, I.G., Scotney, P.D., and Teh, T. (1999). Turn up the HEAT. Structure *7*, R91–R97.

Koyama, M., and Matsuura, Y. (2010). An allosteric mechanism to displace nuclear export cargo from CRM1 and RanGTP by RanBP1. EMBO J. *29*, 2002–2013.

Lapalombella, R., Sun, Q., Williams, K., Tangeman, L., Jha, S., Zhong, Y., Goettl, V., Mahoney, E., Berglund, C., Gupta, S., et al. (2012). Selective inhibitors of nuclear export show that CRM1/XPO1 is a target in chronic lymphocytic leukemia. Blood *120*, 4621–4634.

Matsuura, Y., and Stewart, M. (2004). Structural basis for the assembly of a nuclear export complex. Nature *432*, 872–877.

Maurer, P., Redd, M., Solsbacher, J., Bischoff, F.R., Greiner, M., Podtelejnikov, A.V., Mann, M., Stade, K., Weis, K., and Schlenstedt, G. (2001). The nuclear export receptor Xpo1p forms distinct complexes with NES transport substrates and the yeast Ran binding protein 1 (Yrb1p). Mol. Biol. Cell *12*, 539–549.

Monecke, T., Güttler, T., Neumann, P., Dickmanns, A., Görlich, D., and Ficner, R. (2009). Crystal structure of the nuclear export receptor CRM1 in complex with Snurportin1 and RanGTP. Science *324*, 1087–1091.

Monecke, T., Haselbach, D., Voß, B., Russek, A., Neumann, P., Thomson, E., Hurt, E., Zachariae, U., Stark, H., Grubmüller, H., et al. (2013). Structural basis for cooperativity of CRM1 export complex formation. Proc. Natl. Acad. Sci. USA *110*, 960–965.

Okada, C., Yamashita, E., Lee, S.J., Shibata, S., Katahira, J., Nakagawa, A., Yoneda, Y., and Tsukihara, T. (2009). A high-resolution structure of the pre-microRNA nuclear export machinery. Science *326*, 1275–1279.

Paraskeva, E., Izaurralde, E., Bischoff, F.R., Huber, J., Kutay, U., Hartmann, E., Lührmann, R., and Görlich, D. (1999). CRM1-mediated recycling of snurportin 1 to the cytoplasm. J. Cell Biol. *145*, 255–264.

Petosa, C., Schoehn, G., Askjaer, P., Bauer, U., Moulin, M., Steuerwald, U., Soler-López, M., Baudin, F., Mattaj, I.W., and Müller, C.W. (2004). Architecture of CRM1/Exportin1 suggests how cooperativity is achieved during formation of a nuclear export complex. Mol. Cell *16*, 761–775.

Radu, A., Blobel, G., and Moore, M.S. (1995). Identification of a protein complex that is required for nuclear protein import and mediates docking of import substrate to distinct nucleoporins. Proc. Natl. Acad. Sci. USA *92*, 1769–1773.

Saito, N., and Matsuura, Y. (2013). A 2.1-Å-resolution crystal structure of unliganded CRM1 reveals the mechanism of autoinhibition. J. Mol. Biol. *425*, 350–364.

Svergun, D.I. (1992). Determination of the regularization parameter in indirect-transform methods using perceptual criteria. J. Appl. Crystallogr. *25*, 495–503.

Svergun, D.I. (1999). Restoring low resolution structure of biological macro-molecules from solution scattering using simulated annealing. Biophys. J. *76*, 2879–2886.

Svergun, D.I., and Kozin, M.B. (2001). Automated matching of high- and low-resolution structural models. J. Appl. Crystallogr. *34*, 33–41.

Svergun, D., Barberato, C., and Koch, M.H.J. (1995). CRYSOL - a program to evaluate x-ray solution scattering of biological macromolecules from atomic coordinates. J. Appl. Crystallogr. *28*, 768–773.

Turner, J.G., Dawson, J., and Sullivan, D.M. (2012). Nuclear export of proteins and drug resistance in cancer. Biochem. Pharmacol. *83*, 1021–1032.

Van Der Spoel, D., Lindahl, E., Hess, B., Groenhof, G., Mark, A.E., and Berendsen, H.J. (2005). GROMACS: fast, flexible, and free. J. Comput. Chem. *26*, 1701–1718.

Volkov, V.V., and Svergun, D.I. (2003). Uniqueness of ab initio shape determination in small-angle scattering. J. Appl. Crystallogr. *36*, 860–864.